RANS SIMULATION OF JET ACTUATION IN A BOUNDARY LAYER-FLOW USING CHIMERA GRIDS

S. Mahmood, R. Radespiel,Institut für Strömungsmechanik, TU Braunschweig,
Bienroder Weg 3, D-38106 Braunschweig,Germany

ABSTRACT

This paper presents RANS simulation of flow control in a boundary layer flow using Chimera grids. Numerical simulation of inclined jet actuation in a boundary layer flow over a flat plate was carried out using an unstructured flow solver DLR-TAU code. The effect of grid refinement is presented. Numerical results are compared with experiment conducted in a wind tunnel. The effectiveness of generating longitudinal vortices is assessed by the non-dimensional momentum transport coefficient. The results indicate that the method of producing vortical structures in the mainstream flow is quite effective in increasing the near-wall momentum. This can control flow separation that may occur on aircraft wings and turbo machinery applications. The numerical results agree well with experimental data.

Keywords: Jet Actuator, RANS, Chimera

1. INTRODUCTION

It has been demonstrated in the past that embedded longitudinal vortices are very useful to control turbulent flow and separation through changes in the near-wall stress field.[1] Such vortices can be produced by incorporating jet actuator devices, namely the vortex generator jets. The induced longitudinal vortex structure shift high momentum fluid from the outer region of the boundary layer towards the wall.[2] This effect increases the skin friction and can be utilized to prevent flow separation.[3,4]
The detailed experimental campaign was conducted for jet actuation in a boundary layer flow on the flat plate at the Technische Universität Braunschweig.[5]The measurements were performed within the German Flow Control Network.[6] These experiments provide a platform to assess the flow predicted by the Reynolds-averaged Navier-Stokes (RANS) flow solver. In order to judge the efficiency of the jet actuator, the essential flow control parameters are pitch angle α and skew angle β and the velocity ratio λ. The most optimum configuration range for the skew angle is $\beta = 90 - 105°$.[5] In this study the optimum skew angle of $\beta = 90°$ is used.
The current numerical simulations of a round jet actuator at high Reynolds number are carried out as part of M-Fly AeroNext Program within the German Aeronautics Research Program LuFo IV. The DLR TAU-code has been used for the numerical simulations. Evaluation of numerical and experimental results provide deep insight into the flow physics in the vicinity and downstream of the jet actuator.

2. WIND-TUNNEL EXPERIMENTS

The flat plate boundary layer experiment was performed in the low speed wind tunnel of the Institut für Strömungsmechanik, Technische Universität Braunschweig. Detailed flow field velocity measurements were taken in the cross flow planes downstream of the single jet actuator using the Stereoscopic Particle Image Velocimetry (3C2D-PIV) system as explained in.[5] The flat plate has an elliptical edge and is installed at specific distance above the tunnel floor. The single round jet actuator is positioned at distance of $X = 53\delta$ downstream of the leading edge, where δ is the measured boundary layer thickness at jet actuator location. The diameter of the circular jet is $d = 0.073\delta$ and the pitch angle α is defined relative to the model surface. The skew angle β can be adjusted with respect to the free stream direction (see Fig. 1). The measurements carried out with

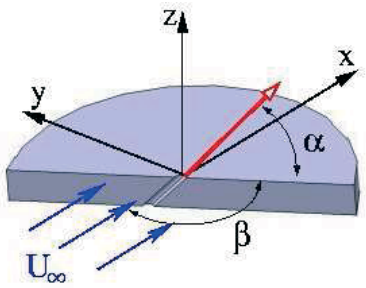

Fig. 1: Schematic of round jet actuator

a free stream velocity of U and distance X results

in a Reynolds number of $Re = 7.67 \times 10^6$. The velocity ratio $\lambda = U_{jet}/U = 2.5$ is used, where U_{jet} is the jet velocity. The assembly of the PIV flow field data normal to the free stream direction at distances $x/\delta = [0.6, 1.2, 2.2, 4.6]$ downstream of the actuator is used to characterize the evolution of the streamwise vortex embedded in boundary layer.

3. NUMERICAL SETUP

The steady state simulations were performed using flow solver code, TAU,[7,8] developed at DLR. TAU-code is a finite-volume based unstructured solver and can be used with both structured and hybrid grids composed of hexahedrons, prisms,tetrahedrons and pyramids. The code provides an option to use chimera grid technique with both structured and hybrid grids, which is useful for complex geometries.[9,10] The inviscid terms in the governing equations were discretized in space using the second-order central scheme with scalar dissipation. In order to improve the convergence of RANS solutions, the TAU-code provides an option of low-Mach preconditioning scheme with multigrid acceleration technique which was used in the numerical simulations. The numerical simulations were computed using a CFL number around unity.

3.1. Chimera Grid

The overlapping grids were constructed with an approach of global and local grids (see Fig.2). This approach has been adopted to handle the large scaling differences between the size of the flat plate and the jet actuator. Furthermore, this methodology allows to alter the structure of the local grids independently of the global grid. The local grid covers the jet actuator and the domain downstream of the jet actuator to capture the vortical structure. The global grid contains the boundaries and limits of the domain. A manual hole cut is used in the global grid to facilitate the local grid at the desired location. The global grid is structured grid here while the local grids used either structured and hybrid grids for the numerical simulations. The local grid is discretized using structured or hybrid grids. The grids were generated using the Gridgen V15[11] package. Fig.3 shows a close up view of the local hybrid grid near the vicinity of the jet actuator.The plan view shows the grid refinement in the lateral direction and also smooth transition of elements from actuator to the farfield. Keeping into account the aspect ratio of elements and avoiding jumps in the element size that lead to convergence problems at boundary layer grid in the jet actuator, the structured grid was first constructed around the boundaries of the actuator and the rest of the domain was then filled with tetrahedrals. The grid points for fine and coarse mesh is 3.7×10^6 and 1.3×10^6 respectively.

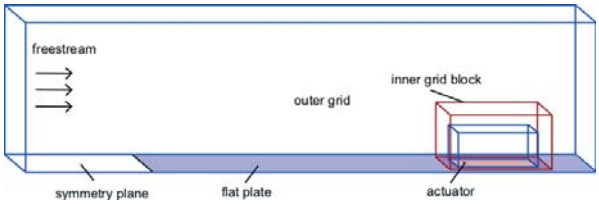

Fig. 2: Non-dimensional layout of the chimera grid for a single round actuator

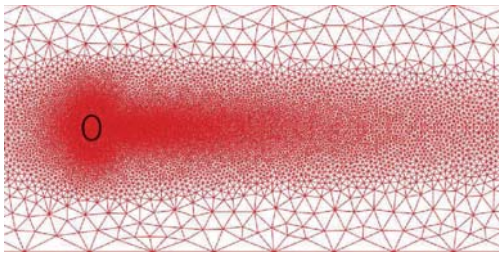

(a) Plan view of the hybrid grid

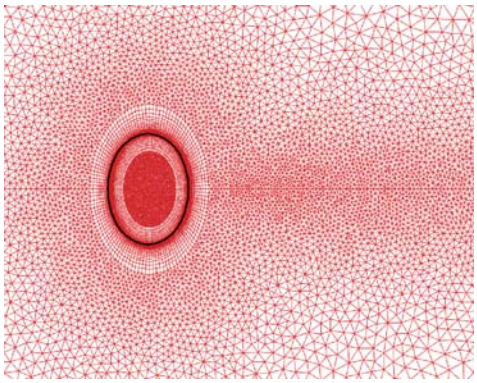

(b) Close up view in the vicinity of the actuator

Fig. 3: Local hybrid grid for single round jet actuator

Similarly, the local structured grid was made in order to see the effect of different grid topology. Fig.4 shows the plan view and the close up view of the local structured grid in the vicinity of the jet actuator. The grid points for fine and coarse mesh is 0.5×10^6 and 3.8×10^6 respectively.

3.2. Turbulence Modelling

The TAU code has various options available for turbulence models. This numerical investigation employs the one-equation turbulence model of Spalart and Allmaras[12] (SAO) and the two-equation $k - \omega$ Shear Stress Transport (SST) model of Menter.[13] The SAO model is famous due to its ease of implementation, relatively low computational expenses, and good performance. The SST model is a $k - \omega$ two-equation model which accounts for the transport

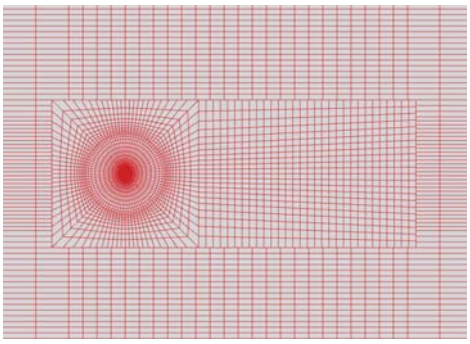

(a) Plan view of the structured grid

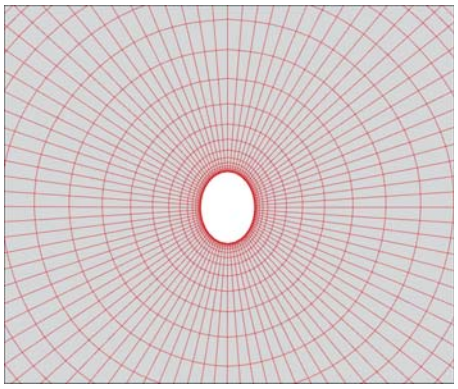

(b) Close up view in the vicinity of the actuator

Fig. 4: Local structured grid for single round jet actuator

of the principal shear stress in adverse pressure gradient boundary layers. Both models are well known and are currently used in aersopace flow simulations.

4. RESULTS

The numerical simulation of skewed jet actuator on a flat plate are performed and compared with the three component PIV measurements in planes downstream of the jet actuator. For the experiment and the numerical simulations, the single jet actuator with a pitch angle $\alpha = 45°$ and skew angle $\beta = 90°$ is investigated.

4.1. Grid Convergence

The effect of grid refinement is studied for the numerical simulations using SAO and SST models. The sensitivity of the grid is investigated downstream of the jet actuator using the streamwise velocity profiles at three wall-normal positions $z/\delta = [0.058, 0.12, 0.23]$. The structured and hybrid grids are labelled as hex_coarse, hex_fine, hybd_coarse and hybd_fine in the plots. Fig.5 shows the streamwise velocity profiles downstream of the jet actuator at $x/\delta = 0.6$. The numerical results show that SAO and SST model predict a complex vortical flow behavior. At wall-normal position of $z/\delta = 0.058$ both SAO and SST give approximately the right position of the vortex core. But none of these models have produced really the bending characteristic of the streamwise vortex, as seen for $z/\delta = [0.12, 0.23]$. The numerical results show that the increase in number of grid points in the wake of the vortex core in streamwise and spanwise direction produced very small change in the results. Fig.6 and Fig.7 shows the streamwise velocity profiles further downstream of the jet actuator. The numerical results seems to be too diffusive as the distance downstream of the jet actuator increases. In this respect the SST model predicts the streamwise velocity profiles better than the SAO model. The results show that the grid refinement has rather little effect in predicting the physics of the longitudinal vortex downstream of the actuator. A closer inspection of the results reveals that the local hexahedral mesh with 3.8×10^6 grid points resolves the complex flow better than the local hybrid grid with 3.7×10^6 points.

4.2. Flow Field

Fig.8, Fig.9, Fig.10 and Fig.11 show the comparison of the streamwise velocity contours downstream of the jet actuator. These figures compare the fine grid numerical results using the SAO and SST turbulence models with the 3C2DPIV experimental data. The velocity contours at $x/\delta = 0.6$ and $x/\delta = 1.2$ in Fig.8 and Fig.9 downstream of the jet actuator show the longitudinal vortex which is less diffused and close to the wall in the experiment than in the numerical simulations. The velocity contours at $x/\delta = 2.2$ and $x/\delta = 4.6$ in Fig.10 and Fig.11 show that the final rate of vortex diffusion between $x/\delta = 2.2$ and $x/\delta = 4.6$ is underpredicted by the CFD results. The numerical simulations obtained by SAO and SST show that initial vortex diffusion is much higher with SAO, while the vertical vortex position is much too high for SAO.

4.3. Influence of Turbulent Eddy Viscosity

In order to further explain the performance of the two eddy viscosity models SAO and SST, contours of the turbulent eddy viscosity and the vorticity magnitude are shown in Fig.12. These contour plots show the streamwise vortex $x/\delta = 0.6$ downstream of the jet actuator. From the contours of vorticity magnitude it can be seen that the peak vorticity is much stronger in the numerical simulations using SST than SAO as flow gradients are much more smoothed with SAO. The contour plots of the turbulent eddy viscosity using SAO and SST are also shown in Fig.12. The SAO model gives a much higher value in the vicinity of the vortex core. The SST model gives a lower

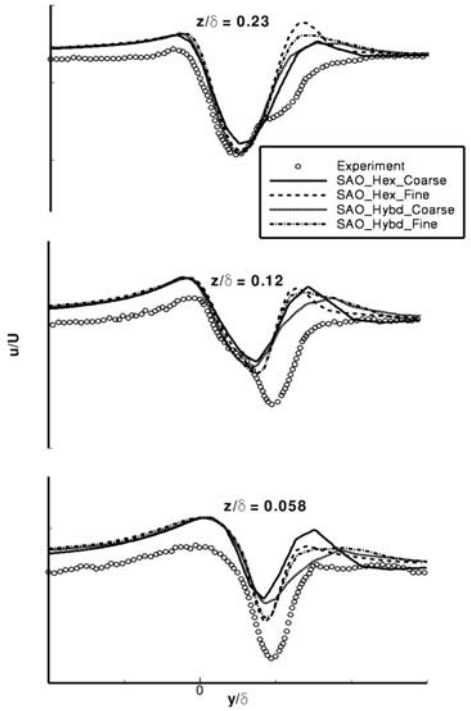

(a) grid convergence SAO

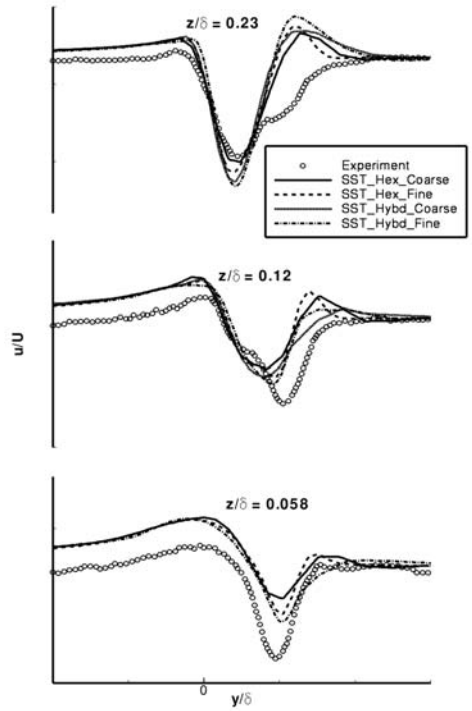

(b) grid convergence SST

Fig. 5: Streamwise velocity predicted by SAO and SST downstream of the actuator, $x/\delta = 0.6$

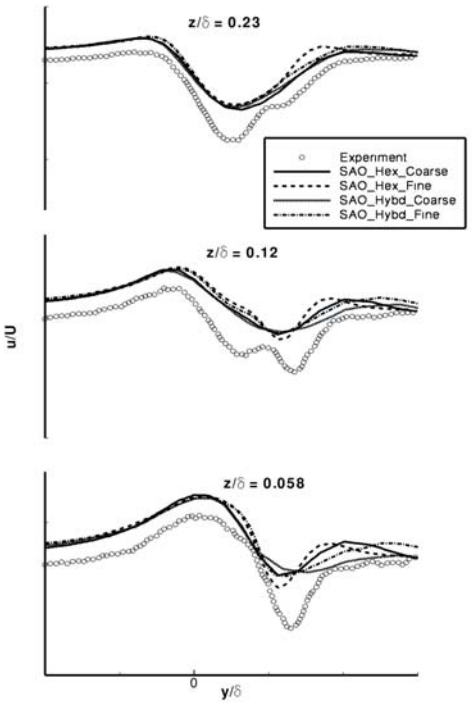

(a) grid convergence SAO

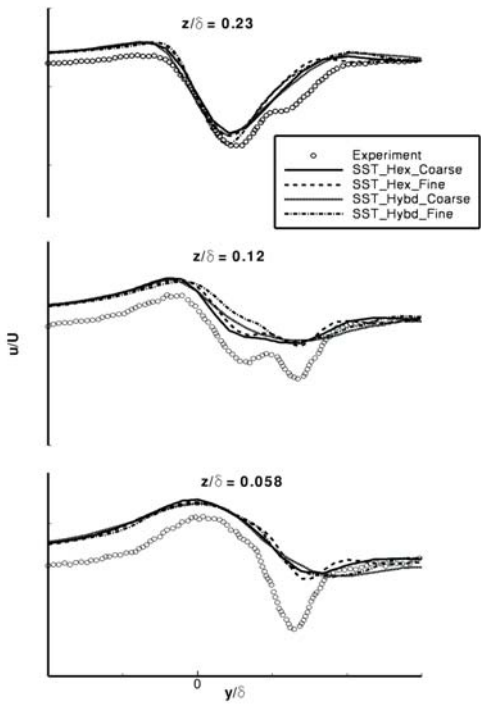

(b) grid convergence SST

Fig. 6: Streamwise velocity predicted by SAO and SST downstream of the actuator, $x/\delta = 1.2$

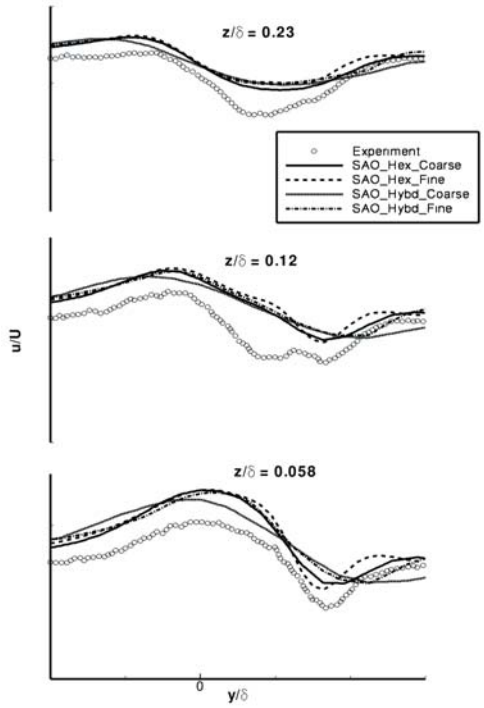

(a) grid convergence SAO

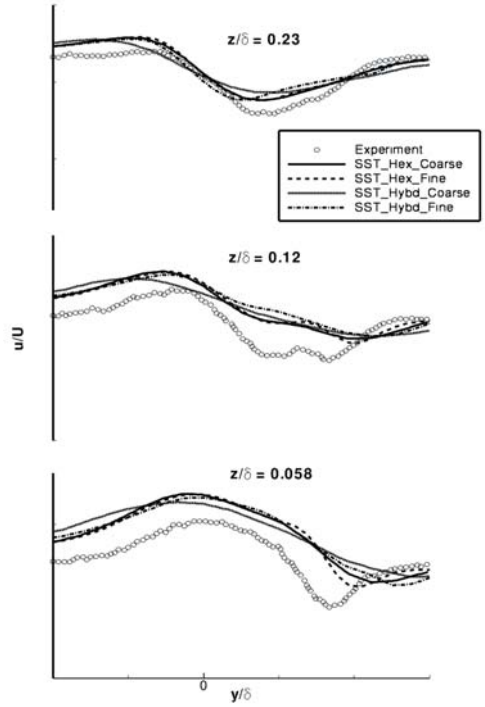

(b) grid convergence SST

Fig. 7: Streamwise velocity predicted by SAO and SST downstream of the actuator, $x/\delta = 2.2$

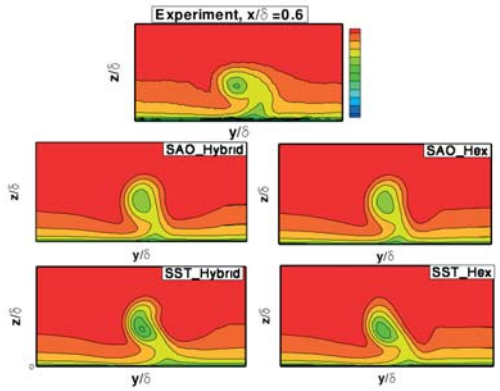

Fig. 8: Streamwise velocity contours, $x/\delta = 0.6$

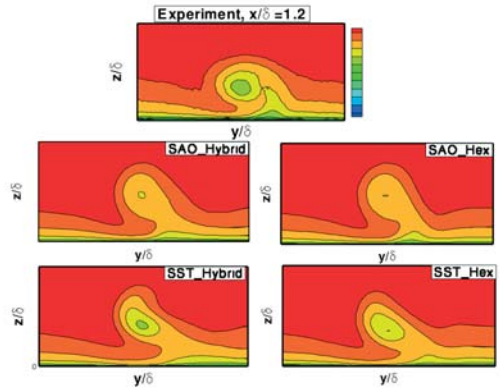

Fig. 9: Streamwise velocity contours, $x/\delta = 1.2$

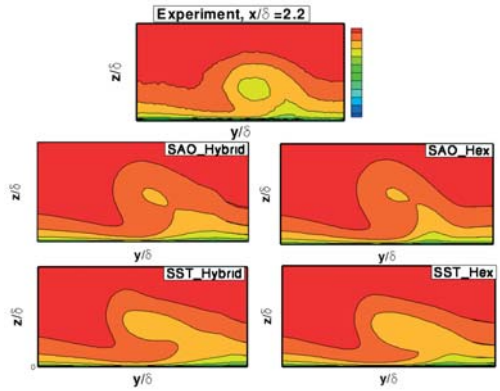

Fig. 10: Streamwise velocity contours, $x/\delta = 2.2$

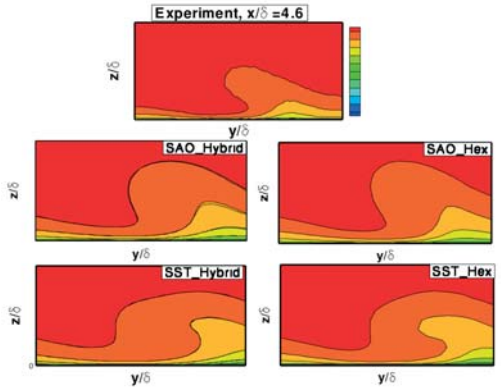

Fig. 11: Streamwise velocity contours, $x/\delta = 4.6$

value near to the vortex core. The higher value of the turbulent eddy viscosity dissipates the peak vorticity in the vortex core.

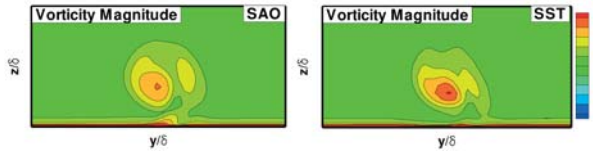

(a) Vorticity magnitude using SAO and SST

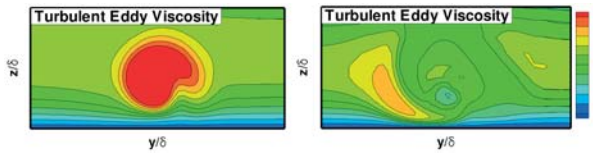

(b) Turbulent eddy viscosity using SAO and SST

Fig. 12: Comparison between SAO and SST using contour plots of vorticity magnitude and turbulent eddy viscosity downstream of the jet actuator at $x/\delta = 0.6$

4.4. Figures of Merit

An estimation of the effect of the induced vortex structure for flow control applications with respect to flow seperation control can be obtained by the determination of figures of merit in the turbulent boundary layer.[14] The figures of merit is a non-dimensional momentum coefficient in streamwise flow direction-x of the flow field. The numerical simulations are compared with the experiment in order to judge the gain in near-wall momentum as induced by the longitudinal vortex in the boundary layer. The figures of merit effected by the induced vortex structure is calculated as given in 1

$$\Delta R_{Vx} = \frac{\int_{y_1}^{y_2} \left[u^2 - u_0^2\right] dy}{\int_{y_1}^{y_2} u_0^2 dy} \tag{1}$$

where ΔR_{Vx} is a non-dimensial momentum coefficient, the $index\ 0$ denotes the undisturbed two-dimensional boundary layer flow and y_1 and y_2 denotes the spanwise lower and upper integration limits for several measuring planes downstream of the jet actuator. The expression characterizes the global momentum tranpsort caused by the longitudinal vortex structure towards the wall.[5] Fig.13,Fig.14,Fig.15 and Fig.16 show the comparison between CFD and PIV measurement for ΔR_{Vx} at several locations downstream of the jet actuator. These figures show that the numerical simulations can predict the momentum increase towards the wall. Fig.13 and Fig.14 show downstream of the jet actuator at x/$\delta = 0.6$, x/$\delta = 1.2$ that the SAO model seems to predict ΔR_{Vx} quite well near the wall. However, the overall trends predicted by the SAO model are not satisfactory. The results obtained using the structured and hybrid grids indicate that SAO model overpredicts the location and growth of the vortex core and the area of deceleration associated with the core. The SST model predicts ΔR_{Vx} reasonably well and the deceleration is in the right position. It appears that the numerical values of SST do not match the experiment very close to the wall. However, we note that the PIV data very close to the wall may suffer from light scattering and vibration in the experiments. Fig.13 and Fig.14 shows that downstream of the jet actuator better results are obtained with structured grid than the hybrid grid. Fig.15 and Fig.16 show that further downstream of the jet actuator x/$\delta = 2.2$, x/$\delta = 4.6$ SAO model diffuses further and overpredicts the vortex core. The SST model predicts the momentum transport due to vortex location and vortex size much better.

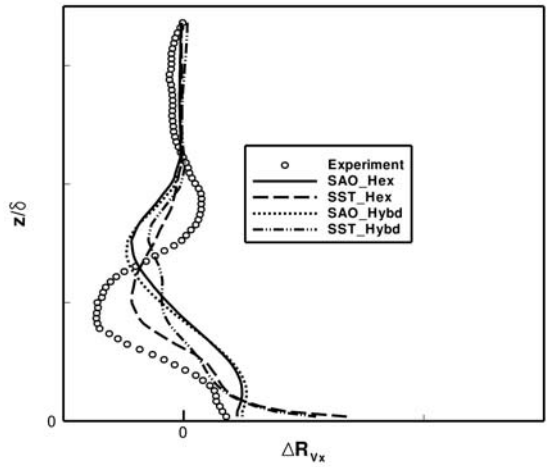

Fig. 13: ΔR_{Vx} comparison between CFD and PIV measurement at $x/\delta = 0.6$

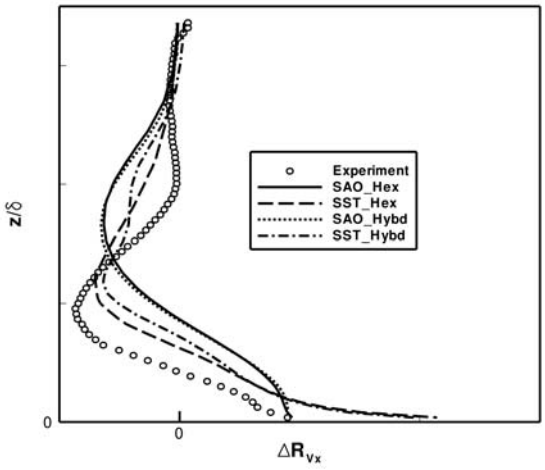

Fig. 14: ΔR_{Vx} comparison between CFD and PIV measurement at $x/\delta = 1.2$

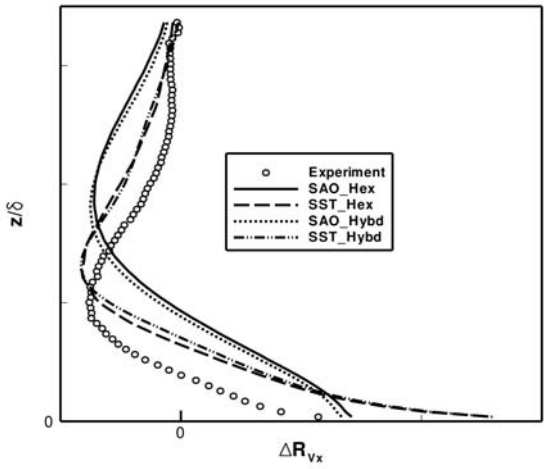

Fig. 15: ΔR_{Vx} comparison between CFD and PIV measurement at $x/\delta = 2.2$

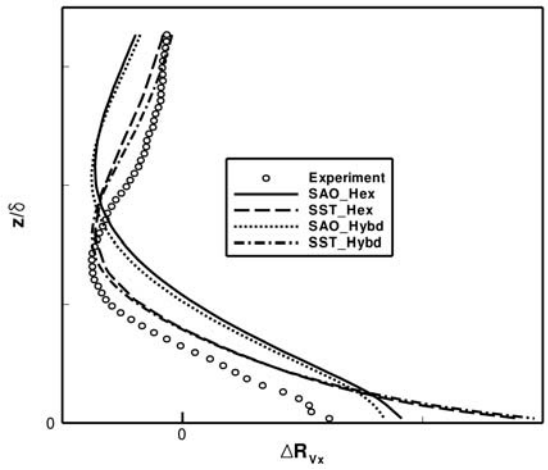

Fig. 16: ΔR_{Vx} comparison between CFD and PIV measurement at $x/\delta = 4.6$

5. SUMMARY

A numerical investigation was carried out on a streamwise vortex structure embedded into the turbulent boudnary layer using a single round jet actuator. The numerical simulations were compared with the existing PIV measurements. It was shown that it is possible to numerically simulate a flow control device like jet actuator using RANS simulations. The grid sensitivity was also investigated. Almost grid independent results were obtained using structured and hybrid grids. Hence the concept of using Chimera grids to resolve the small flow scales associated with the flow actuation was verified. It was shown that the SST model gives better results for vortex induced momentum transport than the SAO turbulence model. The SAO model diffuses the vortex much faster than the SST model. The turbulent eddy viscosity data showed large differences between the SAO model and the SST model. The increase in momentum in near-wall region was determined using a non-dimensional streamwise momentum transport coefficient. Here the SST model was found to reproduce the trends of experimental data, which depend on vortex location in the boundary layer and vortex diffusion in downstream direction. Future investigations should address the question of unsteady vortex motion which has been observed in the experiments.

6. ACKNOWLEDGMENT

The current research was peformed as part of the M-Fly AeroNext Program within the German Aeronautics Research Program LuFo IV. Financial Support by Airbus is gratefully acknowledged. High Performance Computing Resources were made available by HLRN-II.

7. REFERENCES

[1] X. ZHANG, Co and Contrarotaing Streamwise Vortices in a Turbulent Boundary Layer, Journal of Aircraft, September-October 1995, Vol. 32, No. 5, pp. 1095-1101.

[2] J. ORTMANNS, C.J. KÄHLER, Investigation of Pulsed Actuators for Active Flow Control using Phase Locked Stereoscopic Particle Image Velocimetry, 12th International Symposium on Applications of Laser Techniques to Fluid Mechanics, July 12-15, 2004, Lisbon, Portugal.

[3] P.K. CHANG , Control of Flow seperation, Hemisphere Publishing Corporation, 1976.

[4] GODARD AND STANISLAS, G. GODARD AND M. STANISLAS, Control of a decelerating boundary

layer. Part 3: optimization of round jets vortex generators, Aerospace Science and Technology, Vol. 10, 2006, pp. 455-464.

[5] J. ORTMANNS, Aktive Grenzschichtbeeinflussung mittels pneumatischer Wirbelgeneratoren bei grossen Reynoldszahlen, Dissertation ZLR-Forchungsbericht 2009-03 , Technische Universität Braunschweig, Institut für Strömungsmechanik.

[6] J. WILD, G. WICHMANN, F. HAUCKE, I. PELTZER, P. SCHOLZ, Large Scale Separation Flow Control Experiments Within the German Flow Control Network, 2009, AIAA-paper 2009-530.

[7] T. GERHOLD, O. FRIEDRICH, J. EVANS, M. GALLE, Calculation of Complex Three-Dimensional Configurations Employing the DLR-TAU-Code, 1997, AIAA-paper 97-0167.

[8] T. GERHOLD, V. HANNEMANN, D. SCHWAMBORN, On the Validation of the DLR-TAU Code, in W. Nitsche H.-J. Heinemann, R. Hilbig (Eds.), New Results in Numerical and Experimental Fluid Mechanics, Notes on Numerical Fluid Mechanics, 1999, Vol. 72, Vieweg, pp. 426 - 433, ISBN 3-528-03122-0.

[9] A. MADRANE, R. HEINRICH, AND T. GERHOLD, Implementation of the Chimera method in the unstructured hybrid DLR finite volume Tau-Code, October 8-10 2002, 6th Overset Composite Grid and Solution Technology Symposium, Ft. Walton Beach, Florida, USA. http://www.arl.hpc.mil/Overset2002/

[10] A. MADRANE, A. RAICHLE, AND A. STUERMER, Parallel implementation of a dynamic overset unstructured grid approach, July 24-28, 2004, ECCOMAS 2004, Jyväskylä, Finland.

[11] http://www.pointwise.com/gridgen

[12] P. SPALART, AND S. ALLMARAS, A one-equation turbulence model for aerodynamic flows, La Recherche Aerospatiale, 1994, pp. 5-21.

[13] F. MENTER, Improved two-equation turbulence models for aerodynamic flows, 1992, Tech. ReportTM 103975,NASA, NASA Langley Research Center, Hampton, VA 23681-2199.

[14] C.P. TILMANN, K.J. LANGAN, J.G. BETTERTON, AND M.J. WILSON, Characterization of Pulsed Vortex Generator Jets for Active Flow Control, May 8-11, 2000, RTO AVT Symposium Braunschweig, Germany.